J. Wang, W. Xing, X. Huang, X. Jin, H. Yu, J. Wang, L. Song, W. Zeng, Y. Hu (2020) *Smoldering of storage rice: Effect of moldy degree and moisture content*, **Combustion Science and Technology**.
https://doi.org/10.1080/00102202.2020.1813120

Smoldering of storage rice: Effect of moldy degree and moisture content

Jingwen Wang[1#], Weiyi Xing[1#], Xinyan Huang[2], Xin Jin[1], Heng Yu[1], Junling Wang[1], Lei Song[1], Wenru Zeng [1,*], Yuan Hu [1,*]

[1]*State Key Laboratory of Fire Science, University of Science and Technology of China, 96 Jinzhai Road, Hefei, Anhui 230026, China*

[2]*Research Centre for Fire Engineering, Department of Building Services Engineering, Hong Kong Polytechnic University, Hong Kong, China*

[#]**Joint first author**, these authors contributed equally to this study.
***Corresponding author**, to whom correspondence should be addressed.

Abstract

Rice, as one of the most valuable bio-resources, is combustible in nature, which poses an inevitable fire risk for the storage and transport processes. The propensity of rice mold could change the fire hazard and endangers the food security of human beings. In this work, the smoldering spread of normal rice, mildly and severely molded rice were studied under the forced opposed airflow. As the rice molding degree increased, the particle pore surface area increased to enhance the char oxidation. Consequently, the smoldering temperature was higher, the propagation rate became larger, and smoldering was more likely to transition to flame, showing a significant fire hazard and explosion risk. Results also showed that as the moisture content increased, both the smoldering temperature and the propensity to flaming increased, probably because of the increased airflow speed after the expansion of rice particles. This research proves that the molding degree has a significant impact on the fire risk and hazard of rice storage and drying process, thus helping provide a scientific guideline for the safe storage and transportation of rice.

Keywords: *Storage rice; Molding degree; Moisture content; Smoldering spread; Forced airflow.*

1. Introduction

Rice is the most important staple food for the Asian population. For example, China is the largest rice-producing and consuming country in the world, which produced more than 25% of global production (502 million metric tons) in 2017 (Barnes et al., 2013, Tian et al., 2018). With the increase of global urbanization, the demand for rice is expected to rise by another 20% by 2030 (Chen et al., 2016). The increasing rice production and consumption requires a greater capacity for storage and a higher frequency of transport, whereas its fire risk also increases due to the combustible nature of rice. Over the last few decades, the rice storage fires frequently occurred and caused serious damage and economic loss, and many fire incidents started in the form of smoldering combustion (Xie et al., 2020a).

Smoldering is a slow, flameless, low-temperature form of combustion which generates when the oxygen attacks the surface of the condensed phase fuel (Rein, 2014). Generally, the energy required for initiating a smoldering fire is lower (Lin et al., 2019), and most of the smoldering fires start by self-ignition. The dynamics of smoldering combustion has been studied for a wide range of fuels, such as piled dusts (Palmer, 1957, Wu et al., 2015), polyurethane foam (Torero and FernandezPello, 1996), cotton (Hagen et al., 2011, Xie et al., 2020b), and peat (Huang and Rein, 2016b, Huang and Rein, 2019). Smoldering includes three main physicochemical processes, drying, degradation, and char oxidation. The drying process is a robust endothermic course (Yang et al., 2019). The degradation process not only includes the endothermic pyrolysis process but also contains an exothermic oxidation process, depending on the oxygen supply (Huang and Rein, 2016b). The smoldering-to-flame (StF) transition is a widely observed phenomenon (Santoso et al., 2019, Huang and Gao, 2020), which was also observed in rice (Xie et al., 2020a). The moisture content (MC) plays a vital role in the smoldering behaviors, such as the ignition and extinction limit (Huang and Rein, 2016a) and the propensity of StF transition (Santoso et al., 2019).

To date, very few studies have investigated the combustion and fire behavior of grains. Also, there is no industry standard to evaluate the fire hazard of grain storage, except for the protocol of preventing self-ignition. Under improper water control, the proportion of mildew could be more than 5% after harvest. Thus, the vast majority of granaries use chemical agents, such as phosphine, calcium phosphide, ethylene oxide, to fumigate the stored grain and inhibit the bio-activities of grain and microorganisms (Hocking and Banks, 1991, Benhalima et al., 2004, Price, 1985, Daft, 1991). So far, no comparatively complete research is available for the effect of molding degree on the grain combustion process, especially smoldering combustion; thus, there is a knowledge gap.

The primary purpose of this work is to use a simplified bench-scale laboratory apparatus to evaluate the effects of the molding degree of the rice storage on the smoldering fire hazards. Besides, the effects of moisture on smoldering processes also were evaluated. This work may shed light on the combustion behaviors of the rice and other grain products, as well as the fire risk and hazard during the food storage and transport.

2. Experiment methods

2.1. Sample preparation

In this work, the rice samples were collected from the local grain storage in Anhui, China, which has been stored for about a year since 2018. The initial MC of the rice was 9.5%, and another two MCs (12.4% and 15.7%) were obtained by adding distilled water (see the method in the Supplementary Material). To investigate the effect of molding degree, the sample with the 15.7% MC was selected and sealed in a plastic bucket, where the temperature was controlled to 30 °C to accelerate the bio-molding process. After processing for one month, the mildly molded rice (MMR) with the MC of 15.5% was obtained; and after processing for three month, the severely molded rice (SMR) with the MC of 15.4%

was obtained. All these samples were stored in a refrigerator at a constant temperature of 4 °C before the test to allow the water to be absorbed entirely and balanced after the molding process.

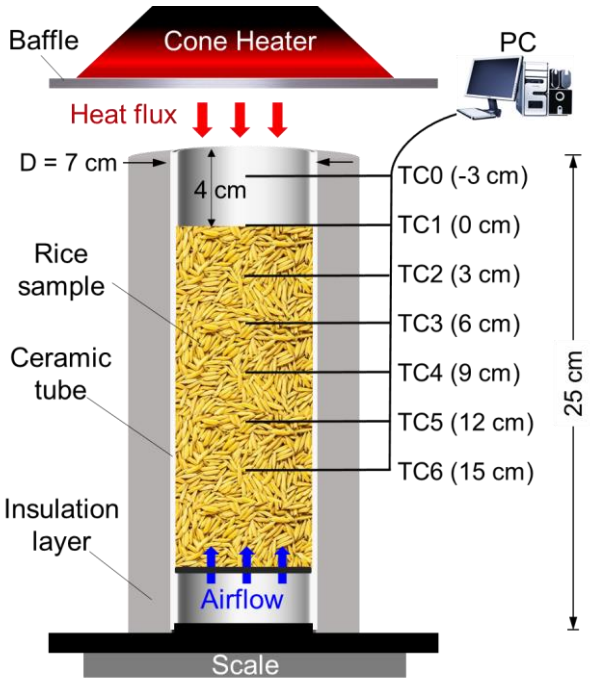

Fig. 1. Schematic diagram of the experimental apparatus.

2.2. Molding degree and chemical components

Table 1 summarizes the major physical parameters and chemical compositions of different rice samples. Although the density and MC are insensitive to the molding degree, the number of spores measured by a microscope significantly increased from 7.8×10^6/g (NR) to 30.9×10^6/g (MMR) and 288×10^6/g (SMR) (Kim and Knudsen, 2016, Jones, 2019). Thus, the number of spores reflects the molding degree, i.e., an key indicator of the quality and safety of grain storage. Measurements showed that the wet bulk density (ρ_{wr}) and dry bulk (ρ_r) density decreased with the molding degree, while the regular pattern of porosity (κ) has an opposite trend.

Table 1. κ (porosity), ρ_{wr} (wet bulk density), ρ_r (dry bulk density), moisture content (MC), free fatty acid (FFA), spores, and main chemical components of all samples.

Sample	κ %	ρ_{wr} (kg/m^3)	ρ_r (kg/m^3)	MC (%)	Spores (10^6/g)	FFA (mg/g)	Starch (%)	Protein (%)	Fiber (%)	Fat (%)	Others (%)
NR	61.3	590	511	15.7	7.8	1.15	58.8	6.0	8.3	2.1	9.1
MMR	61.7	584	506	15.5	30.9	3.83	49.4	6.9	9.4	1.4	17.5
SMR	62.7	583	505	15.4	288.0	4.00	55.5	8.1	12.3	1.3	7.3

For the chemical composition, the free fatty acid (FFA) shows a remarkable increase with the molding degree. As the molding degree increases, the protein content slightly increases from 6.0% to 8.1%, while the fat content decreases from 2.1% to 1.3%, because of the fat hydrolysis in the moldy process and the promoted protein generation by the fungus (Kaya-Celiker et al., 2014, Bartov et al., 1982).

2.3. Smoldering reactor

The schematic diagram of the smoldering reactor is shown in **Fig. 1**. The testing apparatus consisted of five main parts, an electric heater, a ceramic tubular container, thermocouples, an analytical balance, and the air supply system. The cone heater (FTT UK) was placed 65 mm above the sample top surface to provide a constant heat flux (15 kW/m^2), which controlled by the power controller.

The ceramic reactor was wrapped by a 4-cm thick thermal insulation layer to minimize the environmental heat loss. The small cross-sectional area and the long tubular shape (a height of 250 mm and an inner diameter of 70 mm) ensured a vertical smoldering propagation. The rice sample was filled into the tubular container until its top surface was 4 cm below the top surface of the container, and the height of the sample was controlled to 15.5 ± 0.3 cm.

The sample temperature profile was monitored by six embedded K-type thermocouples from TC1 at the top surface (0 cm, TC1) to 15 cm below (TC6) with a 1-mm bead, and the gap between nearby thermocouples was fixed to 30 mm. These thermocouples were able to track the smoldering front and distinguish different smoldering processes (Huang and Rein, 2019). Another thermocouple (TC0) was placed 3 cm above the sample to measure the gas-phase temperature. This TC0 was to distinguish the smoldering and flaming fire, as if the StF transition occurred, the top gas temperature would show a sudden increase. On the bottom of the reactor, there was a steel mesh that could adjust the sample height and ensure the same height in all experiments. The balance below the reactor was used to monitor the sample mass loss during the smoldering process. An air supply system was installed to control upward airflow from the bottom of the sample.

2.4. Experiment procedure

Before the experiment, the sample was weighed 350 g into the reactor. The cone heater power was adjusted to ensure the heat flux to the sample surface to be 15 kW/m^2. Then, the baffle below the heater was removed to expose the fuel bed to the radiation for 2 h to ensure a robust smoldering ignition and propagation. At this time, the upward air supply was controlled to be 0, 5, and 7.5 L/min. Throughout the test, the temperature and mass of rice samples were monitored. In all cases, the experiment was carried out with the top surface open. When temperatures of all thermocouples were below 50℃, the experiment was terminated (i.e., burnout). The SPEX-1403 laser Raman spectrometer (SPEX Co., USA) with excitation provided in backscattering geometry by a 514.5 nm argon laser line and the intensity ratio I_D/I_G was assigned to get the Raman spectra of organized graphitic structures of char. The Brunner−Emmet−Teller (BET) test was also conducted (Micromeritic corporation, U.S.) to characterize the ξ (specific surface area) of the sample.

3. Results

3.1. Failed smoldering without airflow

Fig. 2 shows the temperature evolution inside four different rice samples under the external radiation without any forced airflow. The thermocouple (TC0) 3-cm above the sample top surface is heated by the external radiation to about 250 ℃; thus, no flame occurred during the smoldering ignition process. The close temperature curve of TC0 indicates that the external heating is close for all tests, and the fluctuation is caused by the cooling of airflow.

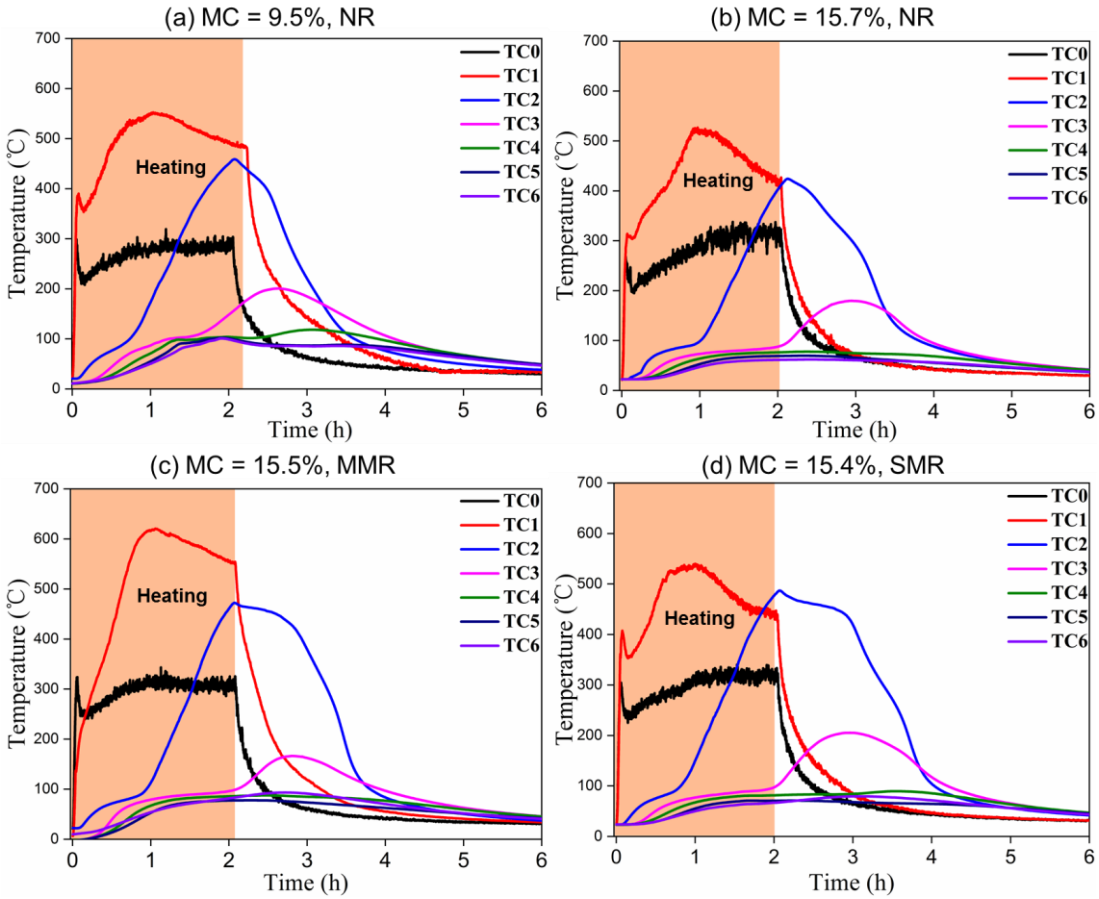

Fig. 2. The temperature evolution of (a) normal rice (NC) with 9.5% MC, (b) NC with 12.4% MC, (c) NC with 15.7% MC, (d) mildly molded rice (MMR) with 15.5% MC, and (e) severely molded rice (SMR) with 15.4% MC.

During the 2-h heating and ignition processes, the temperature on the top surface of rice sample (TC1) and 3 cm below the surface (TC2) exceeds above 450 ℃. Thus, the rice sample has been heated above the threshold temperature of char oxidation and the smoldering ignition temperature of rice, that is, about 300 ℃ (Xie et al., 2020a). The smoldering front has propagated at least 3 cm deep from the top surface. After turning off the cone heater, the overall temperature profile quickly decreases, so that the smoldering process cannot be maintained. Eventually, all samples are cooled down after 6 h. The extinction of smoldering is caused by two reasons, (1) the cooling by the environment and the evaporation process of rice moisture (Lin and Huang, 2020), and (2) the lack of oxygen supply (Zanoni et al., 2019, Xie et al., 2020a). The influence of rice moisture on extinction is relatively small, because the difference between 9.5% MC (Fig. 2a) and 15.7% MC (Fig. 2b) is minor. Thus, the lack of oxygen supply plays a crucial role in the extinction of smoldering (or smothering). A further comparison of **Fig. 2(a-d)** demonstrates that the effect of moisture content and molding degree on the temperature profile for the failure smoldering process is small.

Fig. 3(a) shows the residues of different rice samples after the 2-h smoldering ignition and the following smothering process with respect to the temperature evolution in **Fig. 2**. It is observed that the surface structure of lower MC and molding degree samples is more regular and denser from the digital picture. **Fig. 3(b)** shows the mass loss revolution of different rice samples during the failed ignition process, and **Fig. 3(c)** further compares the mass fraction of residue as a function of rice moisture. The effect of moisture content and moldy degree on carbon residue is similar. Essentially, the larger mass loss fraction of a wetter sample is caused by the evaporation of rice moisture, and the fragile surface structure of moldy samples is a result of lower residues. Specifically, as the MC of NR increased by

about 6% from 9.5% to 15.7%, the residue after heating decreases by about 6% from 71% to 65%. Comparatively, the influence of molding degree on mass loss during the external heating is also negligible. Compare to the NR sample with MC of 15.7%, the slightly increased residues are observed in MMR and SMR, about 0.6 % and 1.2 %, respectively.

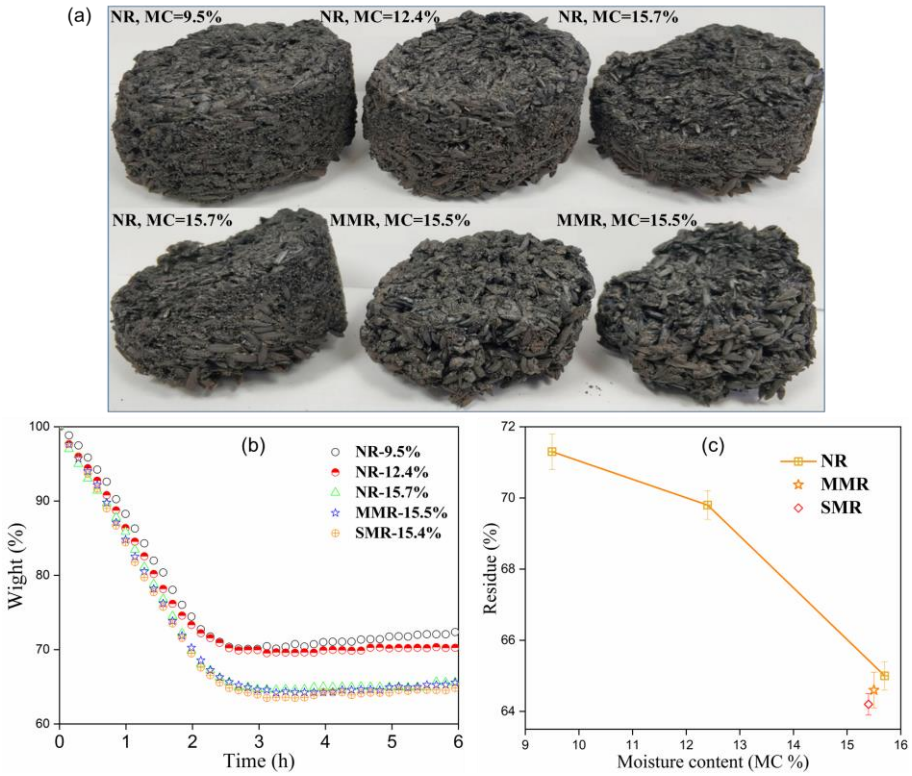

Fig. 3. Sample conditions after 2-h heating without force airflow and failed smoldering ignition, (a) charred rice residue on the top, (2) the mass loss evolution of different samples, and (c) the residue mass fraction vs. MC.

3.2. Smoldering spread with forced airflow

To facilitate the smoldering process, the two opposed airflow rates (5 and 7.5 L/min) were applied from the bottom. **Fig. 4** shows the temperature histories of normal rice (NR) samples with different MC and opposed airflow rates. The measurement of TC0 manifests the heating condition of the cone heater, and a consistent profile of TC0 in different tests indicates that the ignition criterion of smoldering is also consistent. When the MC of normal rice was 9.5%, the applied airflow (either 5 or 7.5 L/min) further sustained a low-intensity smoldering burning of the top 3-cm layer of rice for 2-4 h after the removal of external radiation. However, the smoldering still could not spread downward, because there was only a tiny temperature increase (barely reaching 100 °C) from 6 cm below the top surface (TC3). Thus, the entire burning process stopped after the charring of the top 3-cm layer of rice sample, which was not fully burnout due to a low smoldering temperature.

On the other hand, when the MC increased from 9.5% to 12.4% and 15.7%, the smoldering combustion became self-sustained and successfully spread downward until the bottom of the sample, as seen in **Fig. 4(b-c)**. This result is against intuition because in general, the fuel moisture acts as a heat sink to slow down or prevent the smoldering fire. There is also a conception of maximum moisture content for smoldering, and its value varies from about 10% to 300%, depending on the fuel type and oxygen supply (Zaccone et al., 2014, Huang and Rein, 2017). This abnormal behavior for smoldering rice is likely to be a result of the increasing airflow speed, which is caused by the expansion of the rice particles after absorbing water. Once the rice particle expands, the porosity of the rice bed becomes

smaller, so the airflow speed increases under the same flowrate. Therefore, the airflow speed increases with the increasing MC, and the entire burning duration decreases from about 16 h for 12.4% MC **(Fig. 4b)** to about 11 h for 15.7% MC **(Fig. 4c)**.

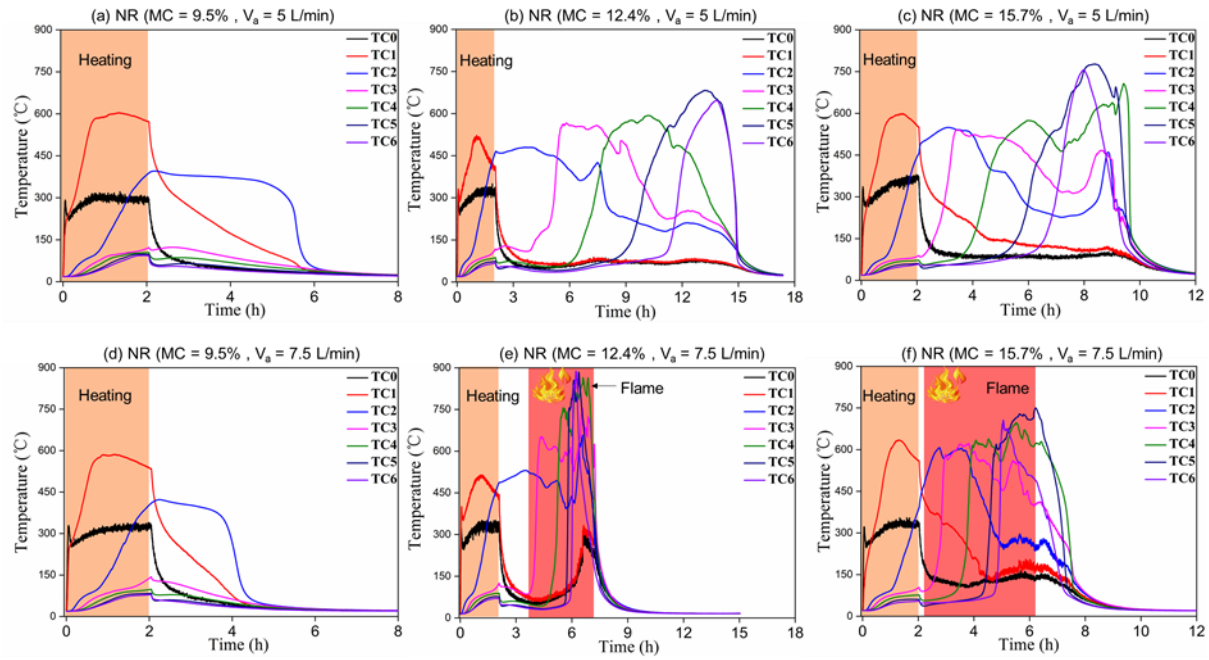

Fig. 4. The temperature histories of normal rice samples (a) 9.5% MC, (b) 12.4% MC, (c) 15.7% MC with the airflow rate of 5 L/min and (d) 9.5% MC, (e) 12.4% MC, and (f) 15.7% MC with the airflow rate of 7.5 L/min, where the red shadow indicating the flaming combustion.

More interestingly, by increasing the flowrate to 7.5 L/min, the smoldering-to-flaming (StF) transition occurs, as seen in **Fig. 4(e-f)**. The occurrence of StF requires a sudden increase of airflow speed, which also supports the explanation of the MC effect here. Once a flame occurs, the additional flame heat flux from the top accelerates the burning of rice. Thus, the burning duration reduces to less than 9 h. Note that after flame occurs, the smoldering combustion continues, because the oxygen supply is from the bottom to the porous rice sample. In other words, the burning is a co-combustion process with both smoldering and flaming, as illustrated in **Fig. 5**. Instead of limiting smoldering, the flame above the sample only provides additional heat flux to facilitate the smoldering combustion. It is different from other natural flaming processes, which may consume all available oxygen to limit or even extinguish the internal smoldering process.

For the smoldering of biomass, generally, there are three reaction fronts: (I) drying front, (II) degradation front, and (III) char-oxidation front, regardless of which chemical model is used (Huang and Rein, 2016b). Once the downward smoldering spread is initiated, the sample is first dried at around 100 °C for an extended period before the fast increase (see **Fig. 4**). Upon the arrival of the char-oxidation front, the peak temperature is reached (He and Behrendt, 2011, Huang and Rein, 2019). Afterward, the high-temperature profile can be maintained due to slow and in-depth char oxidation and the excellent insulation of the ash layer.

Fig. 5(a-d) shows the temporal and spatial temperature histories of samples with different molding degrees and air supply rates. Because all these molded samples have a high MC of 15.5%, the StF transition occurs in all these samples, even when the airflow rate is 5 L/min. Compared to the NR samples in **Fig. 4(c,f)**, the duration of the combustion of the SMR sample is much shorted, and when the flowrate increases 7.5 L/min, the burning duration becomes less than 5 h. Also, the peak combustion

temperature is much higher than NR samples. Both factors imply that the burning of a rice sample with a higher molding degree is much more intensive.

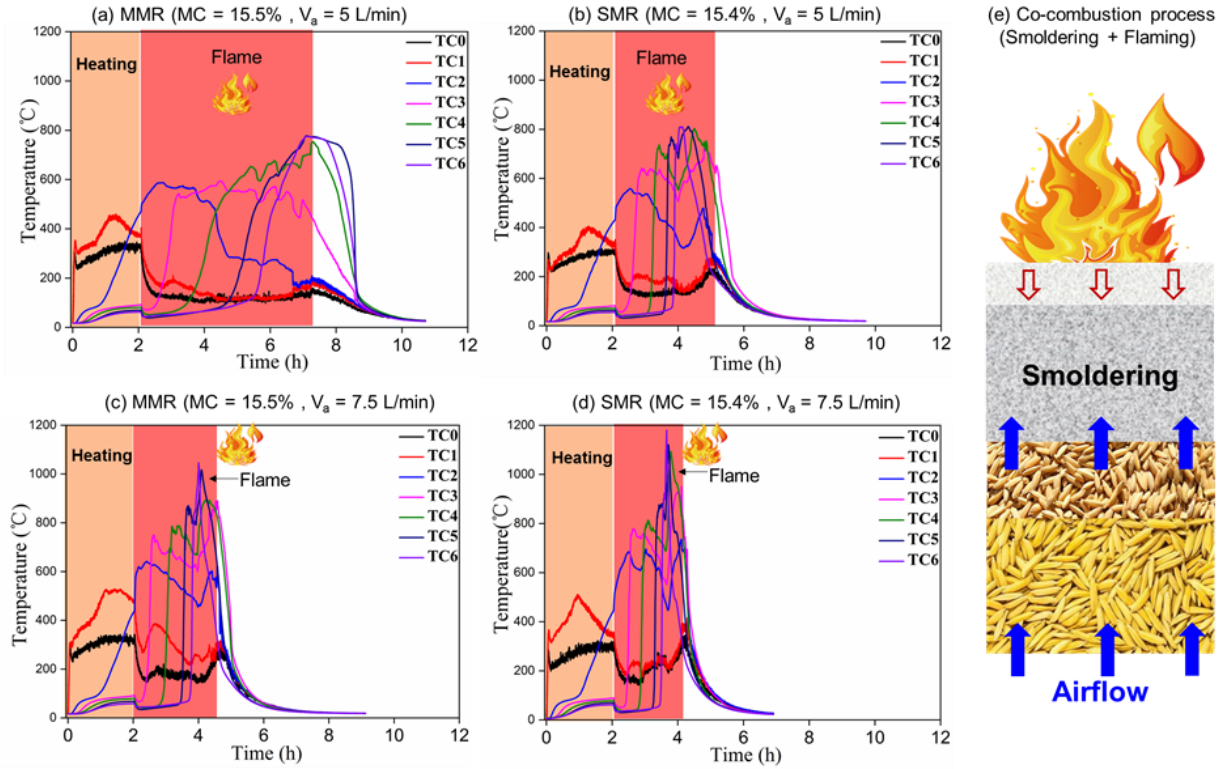

Fig. 5. The temporal and spatial temperature histories of sample MMR with the airflow rate of (a) 5 L/min and (b) 7.5 L/min and SMR with the airflow rate of (c) 5 L/min and (d) 7.5 L/min.

4. Discussions

4.1. Effect of molding on sample's structure

In the actual storage of grain, mildew is often caused by the increase of regional fuel moisture. **Fig. 6(a-b)** shows the N_2 adsorption and desorption isotherms and Raman spectra of the char residues. Both of the samples showed an adsorption isotherm of type IV with a hysteresis of type H3, which indicated an extremely irregular pore structure (Peigney et al., 2001). The ξ (specific surface area) value of low MC was relatively low (18.8 m^2/g) in BET test, while the value increased to 256.4 m^2/g when the rice became severely moldy. The ξ value strongly influenced the heterogeneous reactions, thus affecting the ignitability and the burning rate of solid particles. The higher the porosity offered a larger pore surface area of particles to react with oxygen directly. Therefore, fuel particles with high porosity are more likely to support the smoldering ignition and burn more intensely.

Raman analysis was used to explore the graphitization degree of char residue (Shi et al., 2018, Zhou et al., 2016, Rakotomalala et al., 2010). The Raman results are shown on **Fig. 6(c-d)**. The D band (around 1360 cm^{-1}) only corresponded to amorphous char, while the G band (around 1580 cm^{-1}) was assigned to the organized graphitic structures of the char layer. The intensity ratio I_D/I_G can be called R, corresponding to the microcrystal size of the char layer. A lower value of R (1.0) indicated a larger size of carbonaceous microstructures, which serves as a more protective shield for underlying samples. Hence, it was easy to find that the char of the NR sample was denser than SMR. Such a compact structure resisted the heat and mass transferring into the inner. Meanwhile, this structure was not conductive to the diffusion of the oxygen to the char oxidation zone.

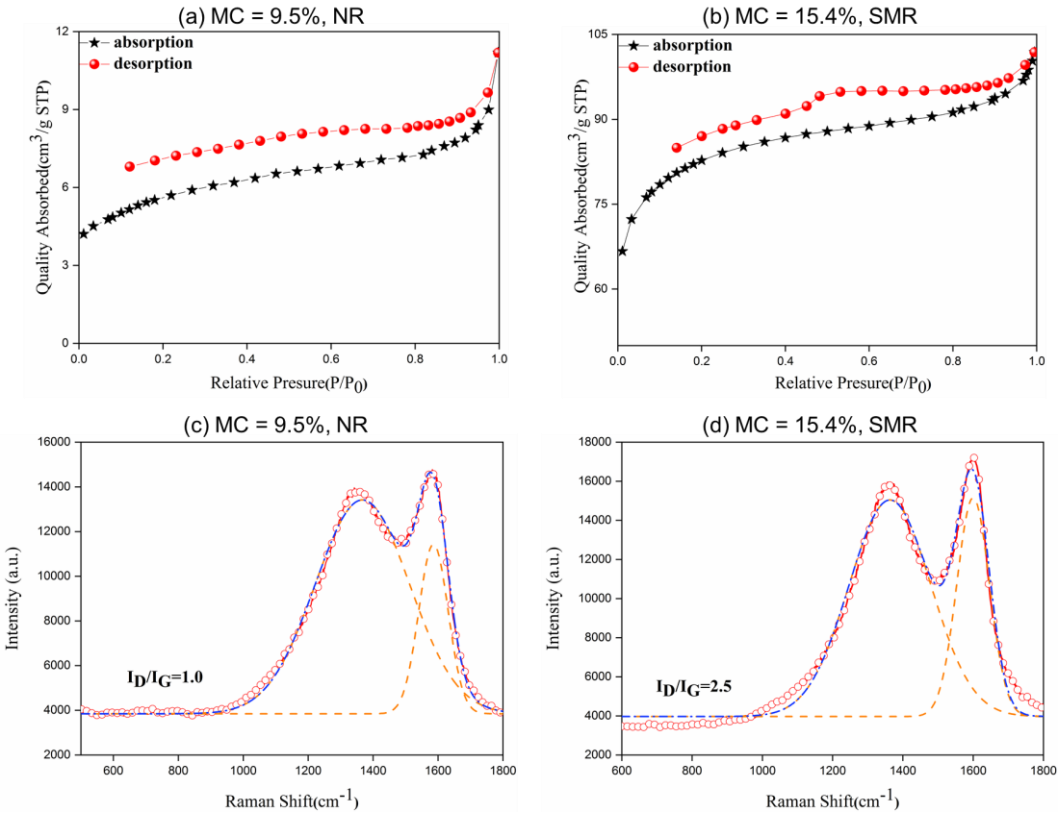

Fig. 6. N_2 adsorption (a) normal rice (NR) with 9.5% MC and (b) severely molded rice (SMR) with 15.4% MC, and desorption isotherms of (c) normal rice (NR) with 9.5% MC and (d) severely molded rice (SMR) after smoldering.

4.2. Maximum temperature

For a burning process, the maximum temperature, as well as the time to reach it reflect the risk and hazard. **Tables S1** and **S2** in the supplementary materials summarize the maximum temperatures measured at each thermocouple location for different MCs and moldy degrees, respectively. Note that a direct comparison among different thermocouples and different tests is meaningless, because some thermocouples measured the flame temperature after the StF transition. To make a fair comparison, we choose the average peak temperature of TC2 and TC3 before they are significantly affected by the flame. **Fig. 7** shows how the maximum smoldering temperature varies with (a) airflow rate and molding degree, and (b) sample moisture.

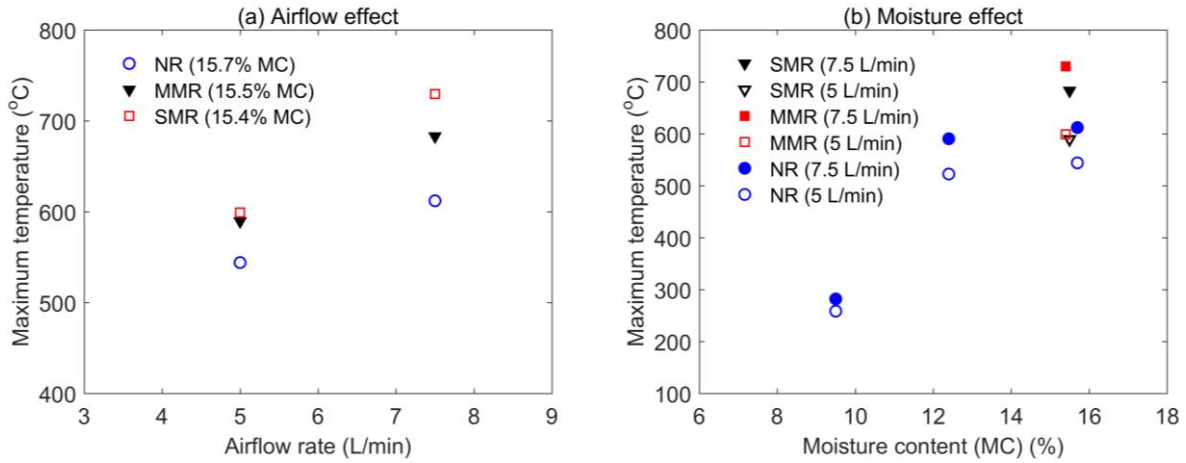

Fig. 7. The maximum smoldering temperature, (a) effect of airflow rate and molding degree, and (b) effect of moisture content.

As expected, the peak temperature increases with the volumetric airflow rate for all samples (**Fig. 7a**). Also, as the molding degree increases, the peak smoldering temperature increases. It is caused by the increase in the particle pore surface area (see **Fig. 6**), which enhances the char oxidation process. On the other hand, as the MC increases from 9% to 15%, the peak temperature also increases (**Fig. 7b**). As discussed before, it is because of the increasing airflow speed after the expansion of rice particles. Note that this trend may not be further extended to a higher MC, where the heat sink effect of moisture could become manifest.

4.3. Rate of smoldering propagation.

The rate of smoldering propagation was calculated from the thermocouple measurement by defining a characteristic temperature, i.e., 250°C (Xie et al., 2020a), for the arrival of the smoldering front (Huang and Rein, 2017). **Fig. 8** summarizes the rate of smoldering for different samples with the airflow rate of 5 L/min. The smoldering speed increases as it gets closer to the bottom inlet of the oxygen, as expected. Similar phenomena have also been observed for the natural smoldering process, where the propagation rate increases when approaching free surface (Huang and Rein, 2019, He and Behrendt, 2011). In addition, once the StF transition occurs, the flaming heating from the top also enhances the smoldering burning inside the sample (see **Fig. 5c**), which also contributes to the acceleration of smoldering propagation. On the other hand, for the SMR sample, the smoldering propagation is the fastest, because the larger particle surface area enhances the char oxidation.

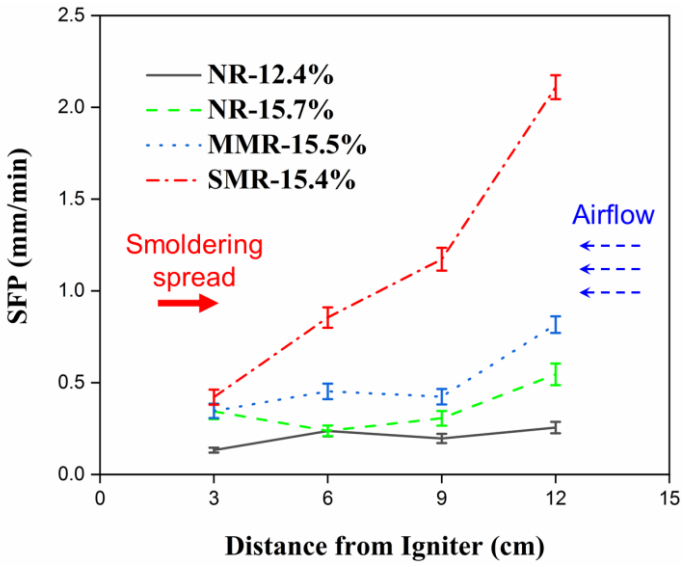

Fig. 8. The velocity of smoldering front propagation (SFP) of different sample with the air flow rate of 5 L/min.

5. Conclusions

As the rice molding degree increased, the particle pore surface area increased to enhance the char oxidation. Consequently, the smoldering temperature was higher, the propagation rate became larger (up to 4 times), and smoldering was more likely to transition to a flame.. Once the transition to flame, the co-combustion process remains with both smoldering and flaming, because the oxygen supply from the bottom is not consumed by the flame. As the moisture content increased, both the smoldering temperature and the propensity to flaming increased. Such a special phenomenon is probably a result of the increased airflow speed, caused by the expansion of rice particle after absorbing the moisture.

Acknowledgments

This work was supported by the National Key Research and Development Program of China [grant number 2017YFC0805900], National Natural Science Foundation of China [grant number 51876183], Youth Innovation Promotion Association CAS (2019448), and Excellent Young Scientist Training Program of USTC (KY2320000018).

References

BARNES, D. G., VIDIASSOV, M., RUTHENSTEINER, B., FLUKE, C. J., QUAYLE, M. R. & MCHENRY, C. R. 2013. Embedding and publishing interactive, 3-dimensional, scientific figures in Portable Document Format (PDF) files. *PLoS One,* 8**,** e69446.

BARTOV, I., PASTER, N. & LISKER, N. 1982. The nutritional value of moldy grains for broiler chicks. *Poult Sci,* 61**,** 2247-54.

BENHALIMA, H., CHAUDHRY, M. Q., MILLS, K. A. & PRICE, N. R. 2004. Phosphine resistance in stored-product insects collected from various grain storage facilities in Morocco. *Journal of Stored Products Research,* 40**,** 241-249.

CHEN, D., TAYLOR, K. P., HALL, Q. & KAPLAN, J. M. 2016. The Neuropeptides FLP-2 and PDF-1 Act in Concert To Arouse Caenorhabditis elegans Locomotion. *Genetics,* 204**,** 1151-1159.

DAFT, J. L. 1991. Fumigants and related chemicals in foods: Review of residue findings, contamination sources, and analytical methods. *Science of The Total Environment,* 100**,** 501-518.

HAGEN, B. C., FRETTE, V., KLEPPE, G. & ARNTZEN, B. J. 2011. Onset of smoldering in cotton: Effects of density. *Fire Safety Journal,* 46**,** 73-80.

HE, F. & BEHRENDT, F. 2011. Experimental investigation of natural smoldering of char granules in a packed bed. *Fire Safety Journal,* 46**,** 406-413.

HOCKING, A. D. & BANKS, H. J. 1991. Effects of phosphine fumigation on survival and growth of storage fungi in wheat. *Journal of Stored Products Research,* 27**,** 115-120.

HUANG, X. & GAO, J. 2020. A Review of Near-Limit Opposed Fire Spread. *Fire Safety Journal*.

HUANG, X. & REIN, G. 2016a. Interactions of Earth's atmospheric oxygen and fuel moisture in smouldering wildfires. *Science of the Total Environment,* 572**,** 1440-1446.

HUANG, X. & REIN, G. 2016b. Thermochemical conversion of biomass in smouldering combustion across scales: The roles of heterogeneous kinetics, oxygen and transport phenomena. *Bioresource Technology,* 207**,** 409-421.

HUANG, X. & REIN, G. 2017. Downward Spread of Smoldering Peat Fire: the Role of Moisture, Density and Oxygen Supply. *International Journal of Wildland Fire,* 26**,** 907-918.

HUANG, X. & REIN, G. 2019. Upward-and-downward spread of smoldering peat fire. *Proceedings of the Combustion Institute,* 37**,** 4025-4033.

JONES, C. J. J. M. M. S. 2019. Crowd Sourced Taxonomic Identification Guide for Categorization and Quantification of Fungal Spores by Optical Microscopy. 2**,** 1-9.

KAYA-CELIKER, H., MALLIKARJUNAN, P. K., SCHMALE, D. & CHRISTIE, M. E. 2014. Discrimination of moldy peanuts with reference to aflatoxin using FTIR-ATR system. *Food Control,* 44**,** 64-71.

KIM, T. G. & KNUDSEN, G. R. 2016. Comparison of plate count, microscopy, and DNA quantification methods to quantify a biocontrol fungus. *Applied Soil Ecology,* 98**,** 285-288.

LIN, S. & HUANG, X. 2020. Quenching of Smoldering: Effect of Wall Cooling on Extinction. *Proceedings of the Combustion Institute (under review)*.

LIN, S., SUN, P. & HUANG, X. 2019. Can peat soil support a flaming wildfire? *International Journal of Wildland Fire,* 28**,** 601-613.

PALMER, K. N. 1957. Smouldering combustion in dusts and fibrous materials. *Combustion and Flame,* 1**,** 129-154.

PEIGNEY, A., LAURENT, C., FLAHAUT, E., BACSA, R. & ROUSSET, A. J. C. 2001. Specific surface area of carbon nanotubes and bundles of carbon nanotubes. 39**,** 507-514.

PRICE, N. R. 1985. The mode of action of fumigants. *Journal of Stored Products Research,* 21**,** 157-164.

RAKOTOMALALA, M., WAGNER, S. & DÖRING, M. J. M. 2010. Recent developments in halogen free flame retardants for epoxy resins for electrical and electronic applications. 3**,** 4300-4327.

REIN, G. 2014. Smoldering Combustion. *SFPE Handbook of Fire Protection Engineering,* 2014**,** 581-603.

SANTOSO, M. A., CHRISTENSEN, E. G., YANG, J. & REIN, G. 2019. Review of the Transition From Smouldering to Flaming Combustion in Wildfires. *Frontiers in Mechanical Engineering,* 5.

SHI, Y., GUI, Z., YUAN, B., HU, Y., ZHENG, Y. J. J. O. T. A. & CALORIMETRY 2018. Flammability of polystyrene/aluminim phosphinate composites containing modified ammonium polyphosphate. 131**,** 1067-1077.

TIAN, Z., NIU, Y., FAN, D., SUN, L., FICSHER, G., ZHONG, H., DENG, J. & TUBIELLO, F. N. 2018. Maintaining rice production while mitigating methane and nitrous oxide emissions from paddy fields in China: Evaluating tradeoffs by using coupled agricultural systems models. *Agricultural Systems,* 159**,** 175-186.

TORERO, J. L. & FERNANDEZPELLO, A. C. 1996. Forward smolder of Polyurethane foam in a forced air flow. *Combustion and Flame,* 106**,** 89-109.

WU, D., HUANG, X., NORMAN, F., VERPLAETSEN, F., BERGHMANS, J. & VAN DEN BULCK, E. 2015. Experimental investigation on the self-ignition behaviour of coal dust accumulations in oxy-fuel combustion system. *Fuel,* 160**,** 245-254.

XIE, Q., GAO, M. & HUANG, X. 2020a. Fire risk and behavior of rice during the convective drying process. *Fire Safety Journal***,** 103013.

XIE, Q., ZHANG, Z., LIN, S., QU, Y. & HUANG, X. 2020b. Smoldering of high-density cotton bale under concurrent wind. *Fire Technology (in press)*.

YANG, J., LIU, N., CHEN, H., GAO, W. & TU, R. 2019. Effects of atmospheric oxygen on horizontal peat smoldering fires: Experimental and numerical study. *Proceedings of the Combustion Institute,* 37**,** 4063-4071.

ZACCONE, C., REIN, G., D'ORAZIO, V., HADDEN, R. M., BELCHER, C. M. & MIANO, T. M. 2014. Smouldering fire signatures in peat and their implications for palaeoenvironmental reconstructions. *Geochimica et Cosmochimica Acta,* 137**,** 134-146.

ZANONI, M. A. B., TORERO, J. L. & GERHARD, J. I. 2019. Delineating and explaining the limits of self-sustained smouldering combustion. *Combustion and Flame,* 201**,** 78-92.

ZHOU, K., GUI, Z. & HU, Y. 2016. The influence of graphene based smoke suppression agents on reduced fire hazards of polystyrene composites Part A Applied science and manufacturing.

J. Wang, W. Xing, X. Huang, X. Jin, H. Yu, J. Wang, L. Song, W. Zeng, Y. Hu (2020) *Smoldering of storage rice: Effect of moldy degree and moisture content*, **Combustion Science and Technology**.
https://doi.org/10.1080/00102202.2020.1813120

Supplemental Materials

Moisture measurement method

Using the physical properties of water in food, at 101.3 kPa (one atmospheric pressure), the temperature of 101℃-105℃, it shall use volatile method to determine the dry weight loss in sample, including absorbent water, partially crystalized water and substances that are volatile under these conditions. Calculate the moisture content by the weighing values before and after weighting.

Take a flat weighing bottle made of clean aluminum or glass and place it in a drying cabinet at 101℃-105℃. The bottle cap is diagonally supported on the side of the bottle. And repeat drying until the mass difference between the two times does not exceed 2 mg, which is the constant weight. Grind the uniformly mixed samples quickly to a particle size of less than 2 mm. Samples that are not easy to grind should be chopped as much as possible, Weigh 2 g-10 g of samples (nearest to 0.0001 g). Place into this measuring bottle. The sample thickness shall not exceed 5 mm. For the loose sample, the thickness shall not exceed 10 mm. Cover it and after precision weighting, place in the 101℃-105℃ dryer. The cap is obliquely attached to the bottle. After 2 h-4 h drying, cover and take it out. After placing in the dryer and 0.5 h cooling, weight. Then place it in the 101℃-105℃ dryer to dry for about 1 hour. Take it out. After placing in the dryer and 0.5 h cooling, weight. Repeat the above steps till the mass difference of twice before and after shall not exceed 2 mg. That is constant weight.

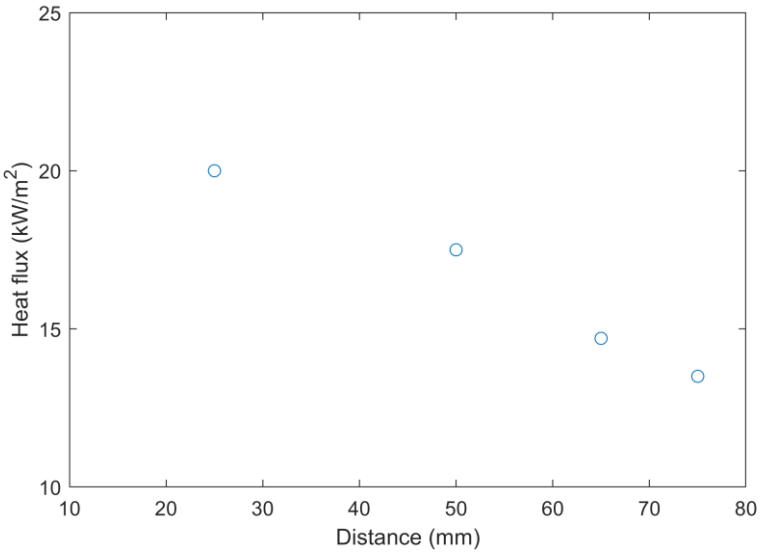

Figure. S1 cone q vs distance.

Figure S2 is the three-dimensional data equivalent temperature plan of time, position and temperature for samples with different air flow rate (5 and 7.5 L/min). It is obviously seen that the smoldering propagated to the inner with time, and we found that the peak temperatures have an evident distinction at the temperature range between 800 to 1100℃. The moisture content and moldy degree, above all, have an obvious influence on the smoldering duration time. With the moisture content and moldy degree increased, the duration time decreased a lot. In addition, the higher the air flow rate, the shorter the duration time.

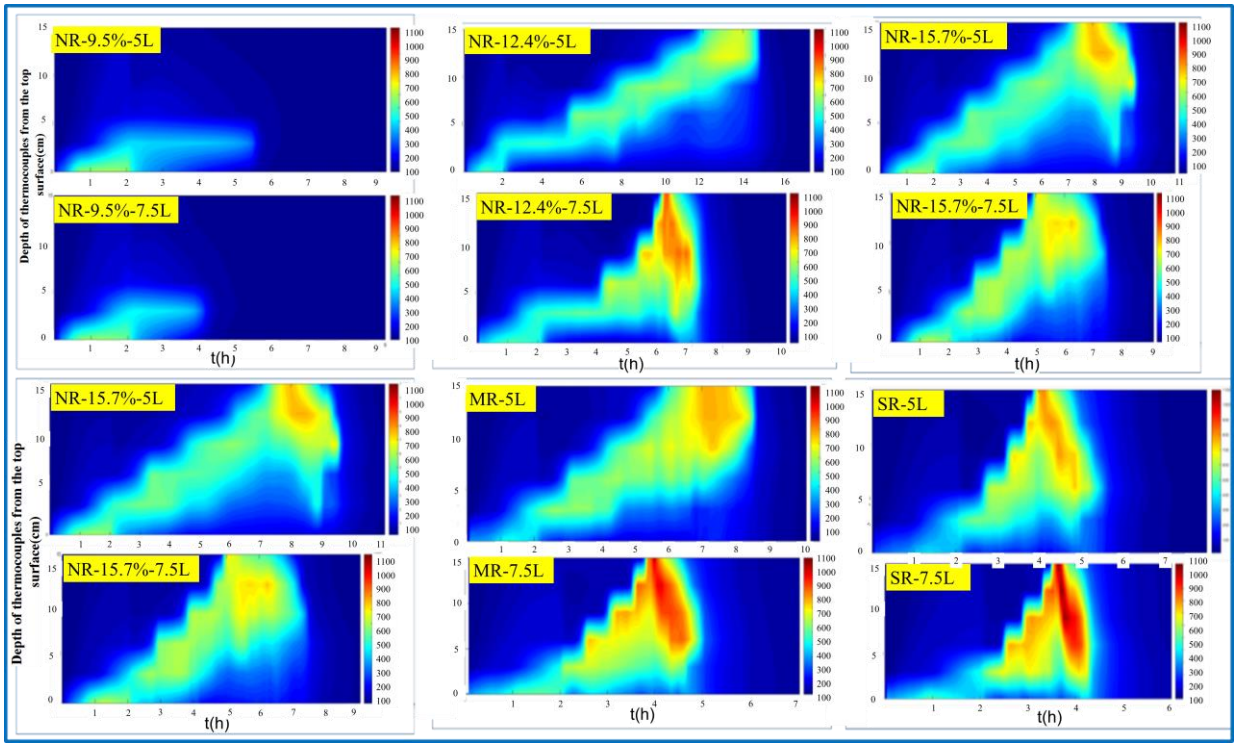

Figure. S2 Three-dimensional data equivalent temperature plan of time, position and temperature for samples with two air flow rates.

Figure. S3 in the supplementary materials shows the digital photos of char residue of different samples after radiation-assisted smoldering combustion without air supply. All of the samples had an evident distinction. The compactness was obviously reduced with the increase of water content and moldy degree.

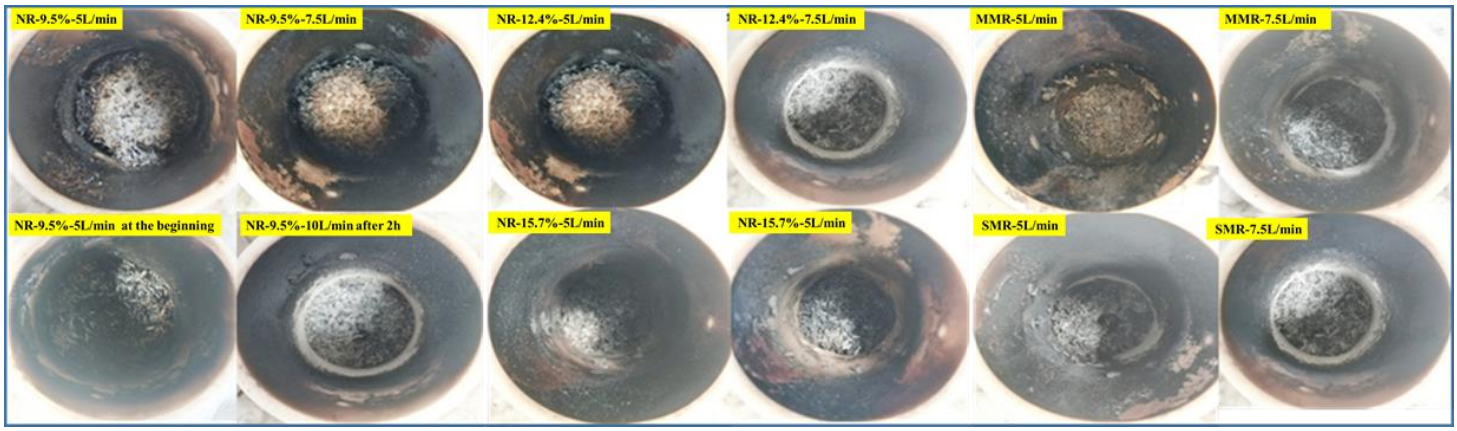

Figure. S3 Char residue of different samples after radiation-aided smoldering combustion with different air supply.

J. Wang, W. Xing, X. Huang, X. Jin, H. Yu, J. Wang, L. Song, W. Zeng, Y. Hu (2020) *Smoldering of storage rice: Effect of moldy degree and moisture content*, **Combustion Science and Technology**.
https://doi.org/10.1080/00102202.2020.1813120

Table S1 The maximum temperature and the time it reached at each location: results for different moisture content sample.

SAMPlES	TC1 (℃)	t1 (h)	TC2 (℃)	t2 (h)	TC3 (℃)	t3 (h)	TC4 (℃)	t4 (h)	TC5 (℃)	t5 (h)	TC6 (℃)	t6 (h)
NR-9.5%-5 L	604	1.25	395	2.16	122	2.05	105	2.05	97	2.05	92	2.05
NR-12.4%-5 L	516	0.98	480	3.71	565	5.85	575	9.20	682	13.2	646	13.7
NR-15.7%-5 L	596	1.46	549	3.06	539	3.46	574	6.01	776	8.34	756	7.96
NR-9.5%-7.5 L	586	1.16	422	2.26	142	2.04	98	2.04	83	2.04	79	2.04
NR-12.4%-7.5 L	513	1.10	530	3.48	651	4.39	752	5.52	853	6.10	884	6.21
NR-15.7%-7.5 L	632	1.26	606	2.73	618	3.49	634	4.07	728	5.62	700	5.05

Table S2 The maximum temperature and the time it reached at each location: results for different moldy degree samples.

SAMPlES	TC1 (℃)	t1 (h)	TC2 (℃)	t2 (h)	TC3 (℃)	t3 (h)	TC4 (℃)	t4 (h)	TC5 (℃)	t5 (h)	TC6 (℃)	t6 (h)
NR-15.7%-5 L	596	1.46	549	3.06	539	3.46	574	6.01	776	8.34	756	7.96
MMR-5 L	449	1.16	586	2.65	593	4.51	648	5.38	778	7.08	775	7.09
SMR-5 L	400	1.24	557	2.53	641	2.89	734	3.42	763	3.78	806	4.05
NR-15.7%-7.5 L	632	1.26	606	2.73	618	3.49	634	4.07	728	5.62	700	5.05
MMR-7.5 L	525	1.16	616	2.15	750	2.63	786	3.18	870	3.69	1042	4.00
SMR-7.5 L	509	0.93	681	2.47	778	2.65	808	3.08	871	3.48	1186	3.65